List-mode proton CT reconstruction using their most likely paths via the finite Hilbert transform of the derivative of the backprojection

Simon Rit, Rolf Clackdoyle, Jan Hoskovec and Jean Michel Létang

Abstract—**Modern prototypes of proton computed tomography (CT) scanners can measure the energy, the position and the direction of each proton, before and after the scanned object, in a list mode. Each detected proton contributes to an estimate of a line integral along an estimated curved proton path. In this work, we propose a backproject first algorithm based on the two-step Hilbert transform to reconstruct proton CT images. The algorithm takes into account the estimated curved paths. A pixel-specific backprojection is computed from the average measurements of protons which traverse the pixel with the same direction according to the proton path estimates. Our simulations studies show that the algorithm has similar spatial resolution to a previous filtered backprojection (FBP) algorithm for proton CT using most likely paths while being computationally more efficient and able to handle truncated data.**

I. INTRODUCTION

The concept of proton CT was proposed early in the history of CT [1]. From measurements of the energy loss of protons through matter, a reconstructed image can be formed of the relative stopping power (RSP) map of tissues. The main disavantadge of proton CT is its poor spatial resolution which is caused by multiple Coulomb scattering that generates quasi-continuous deflections of the protons in matter. However, the potential of proton CT to improve proton therapy treatment planning has lead to new hardware and software developments to combat the spatial resolution issues.

Much improvement of the spatial resolution in proton CT has been achieved thanks to the use of pairs of position sensitive detectors that record the position and the direction of each proton, once before the scanned object and once afterwards [2]. The acquired list-mode information has the advantage that the most likely path of each proton can be estimated [3] and incorporated into the reconstruction algorithm. This technique substantially improves the spatial resolution over methods that use straight-line models, and several groups are now developing such scanner prototypes. Incorporating the

S. Rit and J.M. Létang are with the Université de Lyon, CREATIS; CNRS UMR5220; Inserm U1044; INSA-Lyon; Université Lyon 1; Centre Léon Bérard, France (e-mail: simon.rit@creatis.insa-lyon.fr).

R. Clackdoyle is with the laboratoire Hubert Curien, CNRS and Université Jean Monnet (UMR 5516), Saint Étienne, France.

J. Hoskovec is with the laboratoire Hubert Curien, CNRS and Université Jean Monnet (UMR 5516), Saint Étienne, France and Université de Lyon, CREATIS; CNRS UMR5220; Inserm U1044; INSA-Lyon; Université Lyon 1; Centre Léon Bérard, France.

most likely path in an iterative reconstruction algorithm is straightforward since it can be accounted for in the projection matrix (see, e.g., [4]). However, the practical applicability of iterative reconstruction is limited by the computational time, particularly for some clinical applications such as image guided proton therapy.

Use of proton list-mode data in FBP algorithms is typically performed after binning the data into a set of projection images. It has long been considered impossible to account for curved proton paths since all protons binned together have followed different paths. Therefore, the most likely path was first used with FBP to only include the protons that had followed close to straight paths [5] but it is preferable to make use of all acquired data.

There is no exact analytic reconstruction from integrals along randomly curved lines, but heuristic use of most likely paths of protons in FBP algorithms has recently been demonstrated. First, Rit *et al.* proposed the *distance-driven binning* [6] where multiple projection images per source position are binned using different approximations of proton paths by straight lines. For each of these projections, the straight lines are defined by the same source point but a different point along the most likely proton paths, at the intersection with planes parallel to the detector at different distances from the source. The most likely path of each proton is then indirectly accounted for by using a different set of input projection images for the reconstruction of each voxel using the Feldkamp algorithm [7]. The improvement of the spatial resolution of reconstructed images is similar to what is obtained with an iterative least-square algorithm using curved most likely paths at a much lower computational cost [4].

More recently, Poludniowski *et al.* have proposed another FBP algorithm that more directly uses the most likely paths by switching the order of the filtering and the backprojection [8]. The list-mode data are used to compute the discrete backprojection by averaging the measurements of protons that went through the same voxel with the same direction. The problem of this switching is that the backprojection should theoretically be computed on an infinite support. Since the backprojection array must inevitably be truncated in practice, some low frequency artifacts might be introduced by this procedure.

In this work, we follow a similar approach to that of [8] using another *backproject first* algorithm. Zeng derived a two-dimensional (2D) reconstruction algorithm [9] from the two-step Hilbert transform method [10] that starts with weighted

backprojections. As he pointed out, this property is useful with list-mode data such as those acquired by proton CT scanners. We applied this algorithm to proton CT and investigated its performance on phantom and patient simulations.

II. METHOD

We start with a brief description of Zeng's reconstruction method before deriving an algorithm for its use in proton CT.

A. Backproject first reconstruction algorithm

Let $p(s, \theta)$ be parallel projections of an unknown 2D function $f(x, y)$ where the coordinates $s \in \mathbb{R}$ and $\theta \in [0, \pi)$ define a line by its signed distance to the origin and its angle with the x-axis, respectively. Noo *et al.* have shown [10] that f can be recovered from p using

$$f(x, y) = H \int_0^\pi \left. \frac{\partial}{\partial s} p(s, \theta) \right|_{s=-x\sin\theta + y\cos\theta} \mathrm{d}\theta \quad (1)$$

with H the inverse Hilbert transform. The resulting algorithm involves (1) taking the derivative of the projections p along s, (2) backprojecting the result and (3) taking the finite inverse Hilbert transform of the backprojection along the x direction.

Zeng proposed inverting the order of the derivative and the backprojection in this formula to obtain a *backproject first* type of algorithm [9]. Zeng's formula is

$$f(x, y) = H \left\{ \frac{\partial}{\partial x} b^s(x, y) + \frac{\partial}{\partial y} b^c(x, y) \right\} \quad (2)$$

with the weighted backprojections

$$b^s(x, y) = -\int_0^\pi p(-x\sin\theta + y\cos\theta, \theta) \sin\theta \, \mathrm{d}\theta \quad (3)$$

$$b^c(x, y) = \int_0^\pi p(-x\sin\theta + y\cos\theta, \theta) \cos\theta \, \mathrm{d}\theta. \quad (4)$$

Zeng obtains a reconstruction algorithm consisting of the following steps: (1) calculate two weighted backprojection images b^s and b^c, (2) take the sum of the derivative in orthogonal directions of each backprojection b^s and b^c, and (3) take its inverse Hilbert transform. The next section focuses on how to obtain the two backprojection images b^s and b^c in the context of proton CT.

B. Backprojection for proton CT

We consider an ideal proton CT scanner made of two pairs of flat trackers that record in a list the position and direction of each proton, before entering and after leaving the target object. The energy at the trackers is assumed to be known before the object and is measured after the object. The incidence angle of the protons is varied by rotating the cone-beam source and two pairs of detectors along a circular trajectory.

Protons are deflected many times when going through matter so their overall path is slightly curved. We let $\mathbf{\Gamma}_i(t) \in \mathbb{R}^3$ denote the proton path, with time $t \in \mathbb{R}$ used to parameterize the curved lines and $i \in \{1, ..., I\}$ the proton index in the list-mode data. Using the Bethe-Bloch equation, one can relate the energy loss of the proton to the sum g_i of the three-dimensional (3D) relative stopping power map f of tissues along the proton path $\mathbf{\Gamma}_i$

$$g_i \equiv \int_{E_\mathrm{in}}^{E_\mathrm{out}} \frac{1}{\mathrm{d}E/\mathrm{d}x_w(E)} \, \mathrm{d}E \simeq \int_{t_i^\mathrm{in}}^{t_i^\mathrm{out}} f(\mathbf{\Gamma}_i(t)) \, \mathrm{d}\mathbf{\Gamma}_i(t) \quad (5)$$

with E_in and E_out the energy before and after the object, $\mathrm{d}E/\mathrm{d}x_w$ the stopping power of water, and t_i^in and t_i^out the times at which the proton is measured entering and leaving the patient, respectively. The proton CT reconstruction problem is to obtain an image of f from the path integrals g_i and an estimate $\hat{\mathbf{\Gamma}}_i$ of each proton path, both of which can be obtained from the measurements.
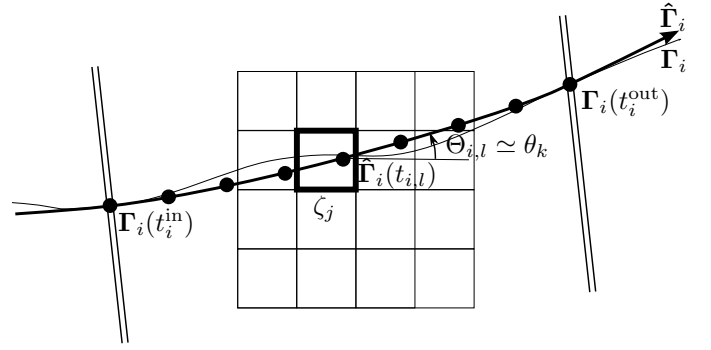

Fig. 1. Illustration of the notation used for the backprojection. The proton follows the path $\mathbf{\Gamma}_i$ and its most likely path $\hat{\mathbf{\Gamma}}_i$ is estimated from its measured positions $\mathbf{\Gamma}_i(t_i^\mathrm{in})$ and $\mathbf{\Gamma}_i(t_i^\mathrm{out})$ and the corresponding directions before entering and after leaving the object, respectively. A discrete set of positions (indexed by l, from $t_i^\mathrm{in} = t_{i,0}$ to $t_i^\mathrm{out} = t_{i,L}$) regularly samples $\hat{\mathbf{\Gamma}}_i$ to evaluate which pixels are reached by the most likely path and the corresponding angle with the horizontal line. For example, here, the position $\hat{\mathbf{\Gamma}}_i(t_{i,l})$ falls in the indicator function ζ_j of the j-th pixel with an angle $\Theta_{i,l}$ that is binned to the closest angle θ_k and contributes to the average measurement $b_{j,k}$ for the j-th pixel and the k-th direction.

Our solution to this reconstruction problem uses Zeng's algorithm which starts by computing the two backprojection images b^s and b^c from the proton data. Only the 2D central slice is considered here but the 3D trajectories of protons are used. Our approach to compute the weighted backprojections is based on [8], i.e., a discretization of Equations 3 and 4. First, we discretize space with $j \in \{1, ..., J\}$ the pixel index of the reconstructed slice. The variable θ is also discretized and we let $k \in \{1, ..., K\}$ be the index of the discrete values θ_k. Finally, the curved most-likely path of each proton is evaluated at a discrete number of time positions $t_{i,l}$ between t_i^in and t_i^out with $l \in \{1, ..., L\}$ the time indices, $t_i^\mathrm{in} = t_{i,0}$ and $t_i^\mathrm{out} = t_{i,L}$ (Figure 1). At each of the positions $\hat{\mathbf{\Gamma}}_i(t_{i,l})$ along the proton paths, we estimate the angle $\Theta_{i,l}$ between the x-axis and the direction of the proton using the proton velocity $\mathrm{d}\hat{\mathbf{\Gamma}}_i/\mathrm{d}t(t_{i,l})$. Using these discretizations, we compute a pixel-specific and direction-specific average of the measurements with

$$b_{j,k} = \frac{\sum_{i,l} \zeta_j(\hat{\mathbf{\Gamma}}_i(t_{i,l})) \xi_k(\Theta_{i,l}) g_i}{\sum_{i,l} \zeta_j(\hat{\mathbf{\Gamma}}_i(t_{i,l})) \xi_k(\Theta_{i,l})} \quad (6)$$

where ζ_j and ξ_k are basis functions for the j-th pixel and the k-th angle θ_k respectively. In this work, the basis functions ζ_j and ξ_k are indicator functions such that each measurement

g_i contributes to the the nearest pixels and directions along the proton path. Therefore, $b_{j,k}$ is the average value of the measurements g_i of protons whose most likely paths traverse pixel j with a direction θ_k.

Recalling that $p(-x \sin \theta + y \cos \theta, \theta)$ is the measurement that corresponds to the line that goes through point (x, y) with an angle θ, images of b^s and b^c are obtained from the average measurements $b_{j,k}$ by discretizing Equations 3 and 4 and summing over the measurements for the same pixel, i.e.,

$$b_j^s = -\sum_k b_{j,k} \sin \theta_k \Delta\theta \tag{7}$$

$$b_j^c = \sum_k b_{j,k} \cos \theta_k \Delta\theta \tag{8}$$

with $\Delta\theta$ the angular gap between consecutive θ_k. From the two discrete images b_j^s and b_j^c, one can reconstruct an image f of the relative stopping power map of tissues using Zeng's algorithm (Equation 2).

III. SIMULATIONS

Proton CT data simulated in previous studies were used to validate the new algorithm. All simulations used Geant4 Monte Carlo simulations [11] performed via Gate [12], the details of which (versions, geometry, physics parameters, etc.) are specified in [6] and [13].
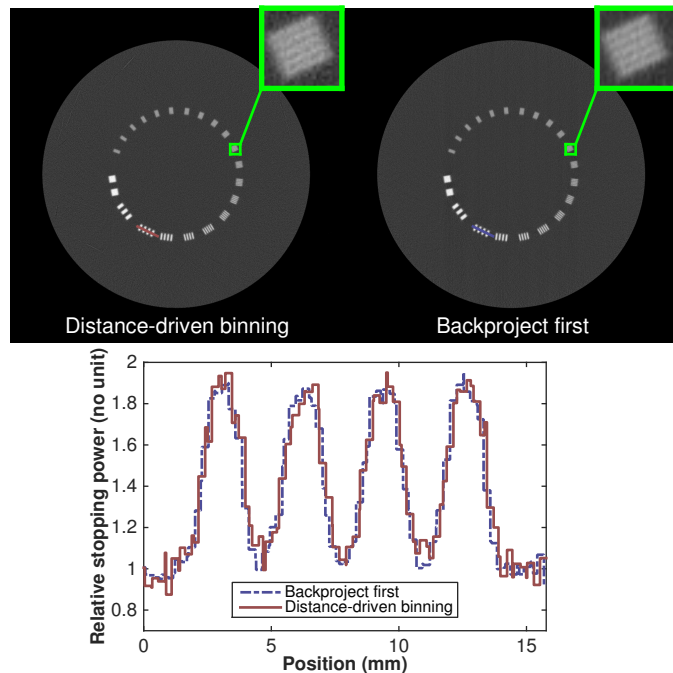

Fig. 2. Slices and profiles of the CTP528 high-resolution module (window $[0.8, 2.0]$). Left: proton CT image obtained with the distance driven binning [6]. Right: proton CT image obtained with the new backprojection-first algorithm. Bottom: profiles along the lines displayed in each reconstruction. The green boxes are zooms in square regions-of-interest.

Two phantoms from [6] were used to evaluate spatial resolution. The first one was a virtual version of the CTP528 high-resolution module of the Catphan phantom (The Phantom Laboratory, Salem, NY) made of a 20 cm-diameter water cylinder with various resolution features along a 10 cm-diameter circle (Figure 2). The second phantom was also a 20 cm-diameter water cylinder with 5 mm cylindrical rods of aluminium at linearly increasing distances from the center of the water cylinder (Figure 3). For these images, there were about $I = 260$ million protons simulated, the reconstructed CT image had $J = 1000 \times 1000$ pixels of 0.25×0.25 mm^2, binned in $K = 720$ directions with $L = 880$ positions taken along each proton path, i.e., about one every 0.25 mm. Each image was compared to the result obtained with the distance-driven binning [6] with the same parameters.
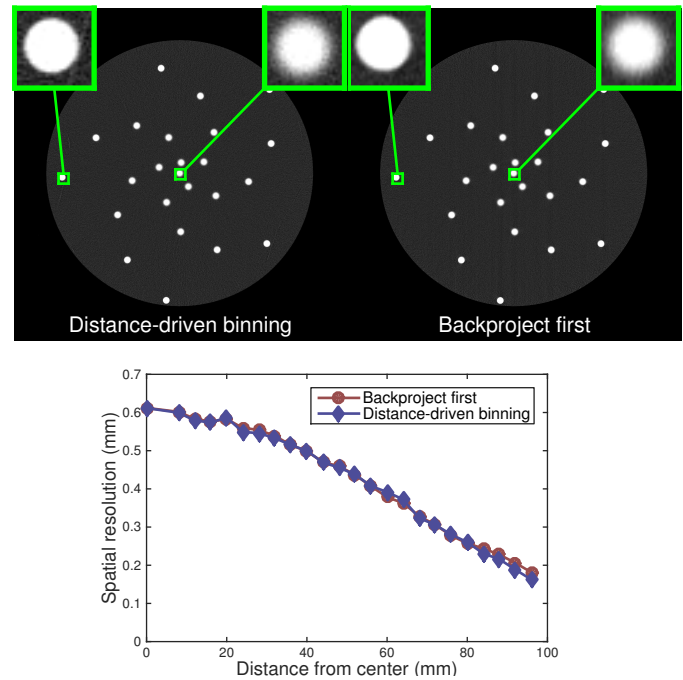

Fig. 3. Slices and spatial resolution measurements of the second spatial resolution phantom (window $[0.8, 2.0]$). Left: proton CT image obtained with the distance driven binning of [6]. Right: proton CT image obtained with the new backprojection-first algorithm. Bottom: spatial resolution of each aluminium insert plot against distance to center. The green boxes are zooms in square regions-of-interest.

The spatial resolution was quantified for each aluminium rod of the second phantom. Radial profiles were taken every degree from the rod center to a distance of 4 mm. A gaussian error function was then fitted to the average profile and its σ value used as a measure of the spatial resolution.

A third simulation was used to illustrate the region-of-interest (ROI) capability of the algorithm, i.e., its ability to reconstruct accurate CT images along segments in the field-of-view (FOV) whose end points were out of the patient. An axial slice of the ICRP phantom [14] was simulated in the lung region in [13]. The detector width was limited to 26 cm at the center-of-rotation. In this case, $I = 3$ million protons were used, the reconstructed CT image had $J = 270 \times 270$ pixels of 1×1 mm^2, binned in $K = 360$ directions with $L = 270$ positions taken along each proton path, i.e., about one every 1 mm.

All the simulations were 3D but the reconstructions were 2D and limited to the axial slice that contains the source trajectory. A slice thickness of 2 mm was used to evaluate if the proton was within the slice but the axial direction was not used otherwise.

IV. Results

The new backprojection-first algorithm gave very similar results to the distance-driven binning method of [6]. The profiles of Figure 2 show different noise patterns but the resolution features are equally visible with both reconstruction algorithms. The quantification of the spatial resolution confirmed these observations (Figure 3). Also, the spatial resolution was better for the rods that were closer to the phantom surface, a behavior that has been observed with iterative reconstruction as well [4] and which can be linked to the difference between the estimated proton path $\hat{\Gamma}_i$ and its real path Γ_i. This difference increased with the distance to the pairs of position-sensitive detectors and was maximal near the center of the scanned object.
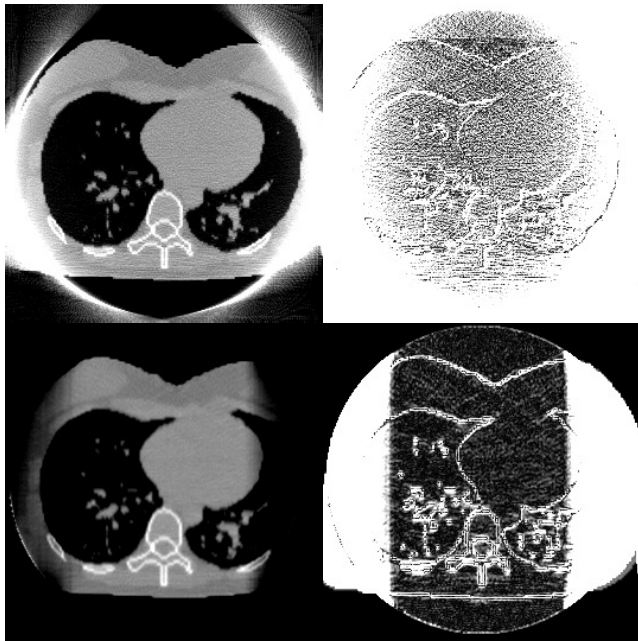

Fig. 4. Reconstructed slices (left, window $[0, 1.5]$) of the ICRP phantom and absolute differences with the reference (right, window $[0, 0.1]$) when the FOV of the scanner is not large enough for the patient. Top: distance-driven binning [6]. Bottom: backprojection-first algorithm proposed in this article. The FOV is a disk whose diameter is visible in the bottom-right image.

One advantage of the new algorithm is its ability to deal with detectors that are not large enough for the scanned object, as illustrated in Figure 4. The differences show that it can accurately reconstruct the vertical segments that are in the field-of-view with both ends in air, whereas no region is accurately reconstructed with the distance-driven binning method.

V. Discussion and Conclusion

The idea of switching the order of the filtering and the backprojection in proton CT, proposed in [8], allows use of the most likely path of each proton during backprojection rather than using an intermediate distance-driven binning before filtering and backprojection [6]. Following the same idea here, we have proposed a different *backproject first* algorithm [9]. However, the new algorithm did not appear to improve the spatial resolution of the reconstructed image compared to the

distance driven binning method, probably because the same most likely path estimation was used in both methods and the difference with the true proton paths is the main source of degradation of the spatial resolution.

The reconstruction time was improved with the new algorithm, for example from 16 s to 3 s for the two reconstructions of Figure 4, excluding the distance-driven binning and the computation of $b_{j,k}$, because filtering is only done once in the image space whereas many sets of projections are filtered in [6]. However, most of the reconstruction time is spent in the computation of the most likely paths which takes a few minutes for both algorithms and would require faster implementations.

The new algorithm is based on the two-step Hilbert transform method [10] and can therefore handle truncated list-mode data (Figure 4). Note that a similar advantage would have been obtained if we had modified the original version in [10] for the use of the distance-driven binning, as was done in [6] with the Feldkamp algorithm. This advantage will be most evident in situations where the detector size is limited, although the proton energy must still be high enough to go through the object in every direction.

References

[1] A.M. Cormack, "Representation of a function by its line integrals, with some radiological applications," *Journal of Applied Physics*, vol. 34, no. 9, pp. 2722–2727, 1963.

[2] R. Schulte *et al.*, "Conceptual design of a proton computed tomography system for applications in proton radiation therapy," *IEEE Trans. Nucl. Sci.*, vol. 51, no. 3, pp. 866–872, June 2004.

[3] R. W. Schulte, S. N. Penfold, J. T. Tafas, and K. E. Schubert, "A maximum likelihood proton path formalism for application in proton computed tomography." *Med Phys*, vol. 35, no. 11, pp. 4849–4856, Nov 2008.

[4] D. Hansen, "Improving ion computed tomography," Ph.D. dissertation, Aarhus University, 2014.

[5] G.A.P. Cirrone *et al.*, "Monte Carlo evaluation of the filtered back projection method for image reconstruction in proton computed tomography," *Nucl Instr Meth Phys Res, Sect A*, vol. 658, no. 1, pp. 78–83, 2011.

[6] S. Rit, G. Dedes, N. Freud, D. Sarrut, and J.M. Létang, "Filtered backprojection proton CT reconstruction along most likely paths," *Med Phys*, vol. 40, no. 3, p. 031103, 2013.

[7] L.A. Feldkamp, L.C. Davis, and J.W. Kress, "Practical cone-beam algorithm," *J Opt Soc Am A*, vol. 1, no. 6, pp. 612–619, 1984.

[8] G. Poludniowski, N.M. Allinson, and P.M. Evans, "Proton computed tomography reconstruction using a backprojection-then-filtering approach," *Phys Med Biol*, vol. 59, no. 24, pp. 7905–7918, Nov 2014.

[9] G.L. Zeng, "Image reconstruction via the finite Hilbert transform of the derivative of the backprojection." *Med Phys*, vol. 34, no. 7, pp. 2837–2843, Jul 2007.

[10] F. Noo, R. Clackdoyle, and J.D. Pack, "A two-step Hilbert transform method for 2D image reconstruction," *Phys Med Biol*, vol. 49, no. 17, pp. 3903–3923, Sep 2004.

[11] S. Agostinelli *et al.*, "Geant4-A simulation toolkit," *Nucl. Instr. Meth. Phys. Res., Sect. A*, vol. 506, no. 3, pp. 250–303, 2003.

[12] S. Jan *et al.*, "GATE V6: a major enhancement of the GATE simulation platform enabling modelling of CT and radiotherapy." *Phys Med Biol*, vol. 56, no. 4, pp. 881–901, Feb 2011.

[13] N. Arbor, D. Dauvergne, G. Dedes, J.-M. Letang, C.-T. Quinones, E. Testa, and S. Rit, "In-silico comparison of x-ray and proton computed tomography for proton therapy dose simulation with a full Monte Carlo treatment planning," in *IEEE Nuclear Science Symposium and Medical Imaging Conference (NSS/MIC)*, 2014.

[14] H.-G. Menzel, C. Clement, and P. DeLuca, "ICRP publication 110. realistic reference phantoms: an ICRP/ICRU joint effort. a report of adult reference computational phantoms," *Ann ICRP*, vol. 39, no. 2, pp. 1–164, 2009.